Scattering of Graphene Plasmons by Defects in the Graphene Sheet

Juan Luis Garcia-Pomar, Alexey Yu. Nikitin,[†] and Luis Martin-Moreno*

Instituto de Ciencia de Materiales de Aragón and Departamento de Física de la Materia Condensada, CSIC Universidad de Zaragoza, E-50009, Zaragoza, Spain. [†]Present address: IKERBASQUE, Basque Foundation for Science, 48011 Bilbao, Spain; CIC nanoGUNE Consolider, 20018 Donostia-San Sebastián, Spain.

ABSTRACT A theoretical study is presented on the scattering of graphene surface plasmons (GSPs) by defects in the graphene sheet they propagate in. These defects can be either natural (as domain boundaries, ripples, and cracks, among others) or induced by an external gate. The scattering is shown to be governed by an integral equation, derived from a plane wave expansion of the fields, which in general must be solved numerically, but it provides useful analytical results for small defects. Two main cases are considered: smooth variations of the graphene conductivity (characterized by a Gaussian conductivity profile) and sharp variations (represented by islands with different conductivity). In general, reflection largely dominates over radiation out of the graphene sheet. However, in the case of sharply defined conductivity islands, there are some values of island size and frequency where the reflectance vanishes and, correspondingly, the radiation out-of-plane is the main scattering process. For smooth defects, the reflectance spectra present a single maximum at the condition $k_p a \approx \sqrt{2}$, where k_p is the GSP wavevector and a is the spatial width of the defect. In contrast, the reflectance spectra of sharp defects present periodic oscillations with period $k_p' a$, where k_p' is the GSP wavelength inside the defect. Finally, the case of cracks (gaps in the graphene conductivity) is considered, showing that the reflectance is practically unity for gap widths larger than one-tenth of the GSP wavelength.

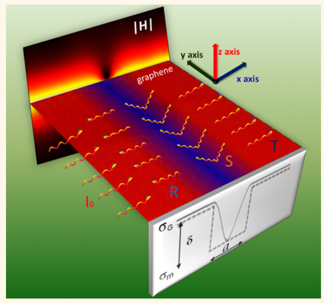

KEYWORDS: scattering · graphene plasmons · conductivity defect · plasmon propagation

In the past few years, it has become evident that graphene not only displays remarkable electronic properties but also plays a significant role in photonics.[1,2] One aspect that has recently attracted much interest is that doped graphene supports bound electromagnetic modes, known as graphene plasmons or graphene surface plasmons (GSPs),[3] which have the appealing characteristics of being both confined in a length scale much smaller than the free space wavelength[4−7] and potentially controllable using external gates. Very recently, the existence of highly confined GSPs has received experimental confirmation.[8−10] Several aspects of GSPs have already been studied theoretically, such as the efficient and directional coupling with nanoemitters (and the associated enhanced spontaneous emission rate),[11−15] enhanced absorption and resonance diffraction,[16−21] metamaterial and antenna applications,[22−24] and their wave guiding capabilities in ribbons[25−30] and edges.[28,31]

However, very little is known about how GSPs behave when they encounter defects in the graphene sheet they propagate in. These defects can occur both (i) naturally as, for instance, kinks appearing due to fabrication process,[32] domain borders in graphene growth by CVD,[33] the presence of multilayer islands,[32] cracks,[34,35] and different domains in CVD graphene;[33] or (ii) created externally, for example, as the changes of conductivity in gate-induced p-n[36] or p-n-p junctions.[37,38]

In this article, we present a theoretical study of GSP scattering by one-dimensional conductivity inhomogeneities. Calculations are conducted with an original method based on the Rayleigh expansion, which has the advantage of providing analytical expressions in some limiting cases.

MODEL

We consider a free-standing graphene monolayer, placed at $z = 0$, with a spatial inhomogeneity in the two-dimensional conductivity σ. Actually, the presence of a substrate may be indispensable for applications, but it does not change any of the fundamental scattering properties of GSPs (affecting mainly the mobility of the charge carriers), which is why in this paper we concentrate on the simplest structure. We will analyze one-dimensional (1D) inhomogeneities, with translational symmetry in the

* Address correspondence to lmm@unizar.es.

Received for review January 22, 2013 and accepted May 15, 2013.

Published online May 15, 2013
10.1021/nn400342v

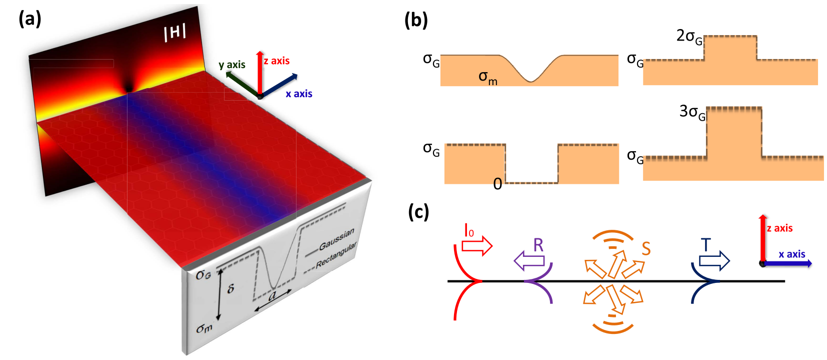

Figure 1. (a) Schematic geometry of free-standing graphene with a defect zone (blue) that interacts with a GSP. The figure shows the conductivity profile (bottom) and a representative case of the computed total (incident + scattered) magnetic field modulus $|H|$ (top). (b) Diagram for the different types of conductivity defects analyzed. (c) Schematics of the scattering processes occurring when a conductivity defect is present in a graphene sheet.

in-plane direction perpendicular to GSP incidence (the y-direction), so $\sigma = \sigma(x)$. The geometry of the system is schematically shown in Figure 1.

Away from the defect, the (frequency-dependent) conductivity of graphene is σ_G. Defects have a characteristic width a and a conductivity σ_m at the defect center ($x = 0$), which can, alternatively, be described by the relative change in conductivity $\delta = (\sigma_m - \sigma_G)/\sigma_G$.

In the scattering geometry, a monochromatic GSP (time dependency $e^{-i\omega t}$), propagating along the Ox axis (from the region $x < 0$), impinges the defect, which induces some reflection back into the SPP channel as well as some radiation out of the graphene sheet. Notice that, due to the symmetry of the problem, all scattered waves have the same polarization as the GSP (transverse magnetic). The scattering amplitudes can be computed by using numerical solvers of Maxwell equations. Here, we present an alternative method, based on the Rayleigh plane wave expansion (RPWE),[39,40] which in general must also be solved numerically but presents the advantage of providing analytical expressions for the scattering coefficients in some limiting cases. We leave all derivations for the Supporting Information and present here the main equations. Within the RPWE method, the electromagnetic field is written (all other components can be readily obtained from Maxwell equations) as

$$E_x(x, z = 0) = e^{iq_p gx} + \int_{-\infty}^{\infty} G(q)B(q)e^{iqgx}dq \qquad (1)$$

where q and q_p are x-components of the wavevectors of a plane wave and GSP, respectively, normalized to the wavevector in vacuum $g = 2\pi/\lambda$. $B(q)$ is the scattering amplitudes, which satisfy the integral equation:

$$B(q) = -\Delta\alpha(q - q_p) - \int_{-\infty}^{\infty} \Delta\alpha(q - q')G(q')B(q')dq' \qquad (2)$$

Here $\Delta\alpha(q)$ is the scattering potential related to the Fourier transform of the inhomogeneity of the dimensionless conductivity $\Delta\alpha(x) = (2\pi/c)(\sigma(x) - \sigma_G)$ and $G(q) = q_z/(1 + q_z\alpha_G)$, where c is the speed of light and $q_z = (1 - q^2)^{1/2}$.

The GSP reflectance and transmittance (R and T, respectively), as well as the fraction of energy flux scattered out-of-plane S, can be obtained from the amplitudes $B(q)$ (see Supporting Information). For instance, $R = |2\pi B(-q_p)/(q_p\alpha_G^3)|^2$.

It must be pointed out that this model does account for losses in the graphene sheet. However, in most cases considered in this paper, the defect size a is much smaller than the GSP absorption length L_p, so the inclusion of losses leaves the scattering coefficients virtually unaltered. The validation of this procedure for small defects through the comparison with calculations performed considering absorption (running simulations with both the RPWE method and a commercial finite-elements code[41]) is presented in the Supporting Information. There we also show that, even for the largest defects considered, the model without losses provides a good starting point for understanding basic properties of GSP scattering. Therefore, and in order to concentrate on the scattering coefficients intrinsically due to the defect, all calculations presented here have been obtained setting $\mathrm{Re}[\sigma_G] = 0$. In this way, current conservation implies $R + T + S = 1$.

Throughout the paper, the conductivity is taken from the RPA expression[42−44] and, for definiteness, we consider that the chemical potential is $\mu = 0.2$ eV. As we will show, this choice is not essential, as most results only depend on μ through the value of the GSP wavevector.

Of course, the scattering coefficients associated with any particular defect will depend on its conductivity profile. Here, we do not attempt to compute this profile; instead, we will assume some basic spatial dependences for the conductivity and compute how they scatter GSPs. We analyze two differentiated main cases: (i) smooth variations in the conductivity, described by a Gaussian profile $\sigma(x) = \sigma_G\{1 + \delta\,\exp(-4x^2/a^2)\}$, where a is the full spatial width at $1/e$ relative conductivity change; and (ii) abrupt ones, represented by a step defect $\sigma(x) = \sigma_G\{1 + \delta\Theta(a/2 - |x|)\}$, where $\Theta(x)$ is the Heaviside step function.

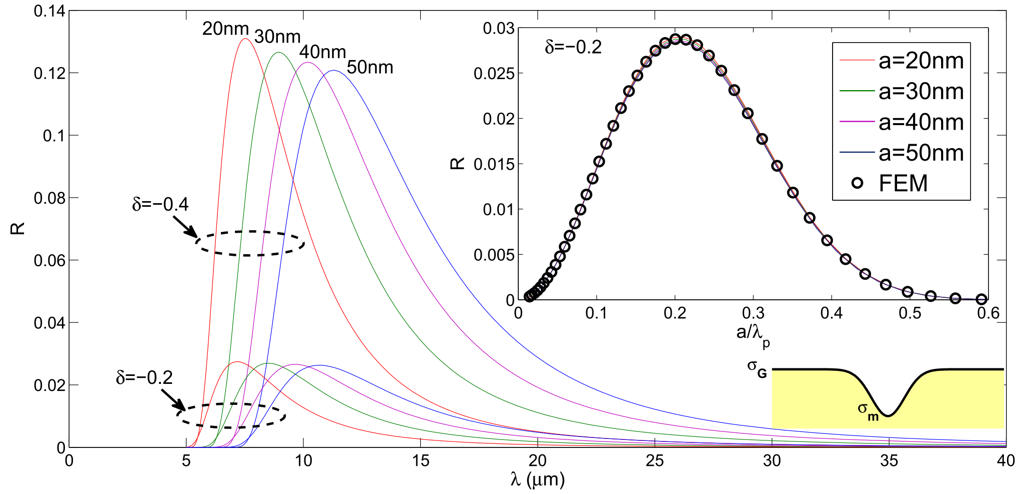

Figure 2. Reflectance spectra $R(\lambda)$ for a GSP impinging a shallow Gaussian conductivity defect, for different defect widths and two values of the relative change in conductivity at the defect center, δ. Inset: R as a function of a/λ_p for $\delta = -0.2$ and different widths, showing that the reflectance scales with a/λ_p. The results obtained with the finite-element method (open circles) for a = 30 nm and $\delta = -0.2$ are also shown, in order to confirm the validity of the RPWE calculations.

RESULTS AND DISCUSSION

Smooth Defects. Let us advance that, for all smooth defects considered, our calculations show that the scattering out-of-plane is extremely small ($S/R \lesssim 10^{-4}$–10^{-2}). This point will be discussed later; now it allows us to focus on the reflectance, from where the transmittance can be obtained as $T \approx 1 - R$.

We first consider a Gaussian profile variation in the conductivity with a small δ. This profile provides a good approximation to the realistic variations on graphene conductivity arising from atomic steps in the substrate when graphene is grown on SiC.[32] In this case, the characteristic width of the Gaussian profile is $a \sim 20$–50 nm, and the conductivity relative change δ ranges between -0.01 and -0.5.

Figure 2 renders the reflectance spectra R for defects with different widths and two values of the relative change in conductivity. We observe that R has a maximum for each value of δ and a. This maximum arises as a compromise between two distinct asymptotic dependencies. For small GSP wavelengths, λ_p, the GSP follows adiabatically the variation of the conductivity and virtually no reflection is generated. Conversely, in the long wavelength region, the defect width is very small in relative terms ($a \ll \lambda_p$) and so is the reflectance, which decreases with λ due to the decrease in a/λ_p. Between these asymptotic decays, there is maximum for R, related to the q-space Fourier image of the Gaussian conductivity profile.

In order to gain more insight into the behavior of the GSP reflectance and to obtain some quantitative estimations to support the exact calculation, we compute the plane wave amplitudes $B(q)$ within the first-order Born approximation (FOBA). This approximation is valid for small variations of δ and corresponds to neglecting the integral term in the right-hand side of eq 2, keeping only the linear term in $\Delta\alpha$.

Within FOBA, the scattering amplitude reads $B^{FOBA}(q) = -\Delta\alpha(q - q_p)$. Using $\alpha_G^{-2} = 1 - q_p^2 \approx -q_p^2$, we obtain (see details in Supporting Information)

$$R^{FOBA} = \frac{\pi}{4}(k_p a)^2 e^{-1/2(k_p a)^2}\delta^2 \qquad (3)$$

Notice that, within the FOBA, the quantity R/δ^2 is a universal function of a/λ_p. It also predicts that the maximum in reflectance occurs when $a/\lambda_p = 1/(\sqrt{2}\pi) \approx 0.22$ (independent of δ), with a maximum reflectance $R_{max}^{FOBA} = (\pi/2e)\delta^2 \approx 0.58\delta^2$. The validity of the scaling of the reflectance with a/λ_p predicted by the FOBA is shown in the inset to Figure 2 for different defect widths and $\delta = -0.2$. Additionally, Figure 3 renders the scaling with δ computed for a narrow defect, together with the prediction by the FOBA. The FOBA captures very accurately the spectral position of the maximum reflectance, even for moderate variations in conductivity, and gives a good approximation to the full reflectance spectra. The FOBA also provides insight into the relative strength of reflectance and radiation channels. The scattering strength depends both on (i) the density of final states (which is much larger for GSPs than for radiation channels) and (ii) a matrix element, given by the Fourier component of the conductivity variation evaluated at the wavevector difference Δk between the GSP one and that of the final state (*i.e.*, $\Delta k = -2k_p$ for reflectance and $\Delta k \approx -k_p$ for radiation processes). In the case of smooth defects, the FOBA shows that the density of states factor dominates over the "matrix element" one (see Supporting Information). Actually, at the reflectance maximum, the FOBA predicts $S/R = 0.5e^{3/4}|\alpha_G|^2$, which is in the range of $\sim 10^{-4}$ to 10^{-2} for the values of α_G relevant for GSP propagation ($\alpha_G \sim 1$–$5\alpha_0$, where $\alpha_0 \approx 1/137$ is the fine structure constant). This preponderance of R over S holds even for larger defects strengths, where the FOBA is no longer strictly applicable.

It is also interesting to analyze the scattering by smooth defects with large δ, as they can be produced

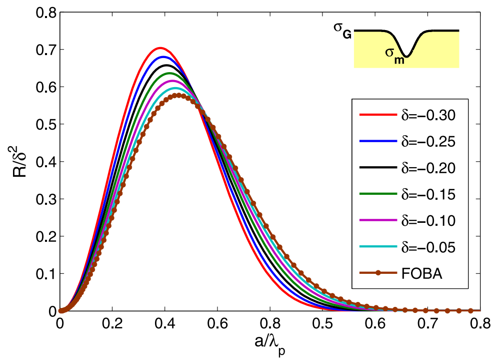

Figure 3. R/δ^2 **as function of** a/λ_p**, for a Gaussian conductivity defect with** a **= 50 nm and different values of the relative change in conductivity at the defect center** δ**. For small** δ**, the curves converge to the universal reflectance spectra predicted by the FOBA, which is still a good approximation for moderate values of** δ**.**

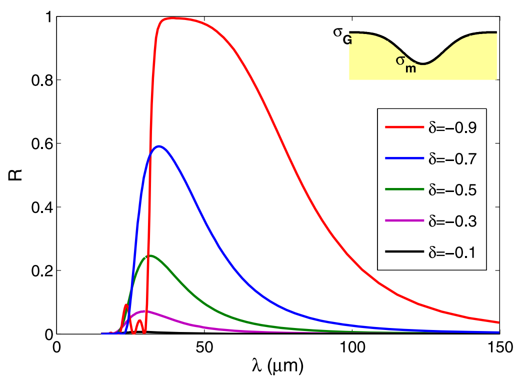

Figure 4. Reflectance spectra for a GSP impinging a Gaussian conductivity defect for different values of δ**, showing the spectral shift of maximum reflectance with relative change of conductivity at the defect center. The defect width is** a **= 400 nm.**

by changing the carrier concentration in graphene (and thus the conductivity) with an external gate.[37,38] The Gaussian shape in this case may simulate a $n^- - n - n^-$ (or $p^+ - p - p^+$) junction. In this case, the defect width will depend on the geometrical details of the gate but can be expected to be on the order of 0.2−1 μm, and δ can be considered a tunable parameter ranging from −1 to 0.

Figure 4 presents the reflectance spectra for different values of δ, for the fixed defect width a = 400 nm. These results show that, for large relative changes of the conductivity, the maximum reflectance occurs for even smaller defect widths than those predicted by the FOBA and that, for large $|\delta|$, there are spectral regions where the reflectivity is high. This point is even more apparent in Figure 5a, which renders the reflectance spectra for δ = −0.9 and different defect widths. Interestingly, the reflectance still satisfies approximately the scaling relation in a/λ_p predicted by the FOBA (see Figure 5b), although for this large value of $|\delta|$ the FOBA is no longer a good approximation to the scattering amplitudes, which must be obtained by solving the full integral of eq 2.

It is remarkable that, for the large relative change in conductivity considered in Figure 5, the reflectance in the spectral region $a/\lambda_p > 0.2$ is small. Actually, there are values of a/λ_p where the reflectance vanishes and, given the scattering out-of-plane is negligible, the transmittance is almost unity. As the GSP extension in the direction perpendicular to the graphene sheet scales with the conductivity, the GSP is very strongly bound at the defect center. Then, unit transmittance and conservation of energy imply that the electric field is strongly enhanced at the center, as illustrated in Figure 6a. The scaling of the electric field amplitude can be obtained by assuming that, for adiabatic propagation of GSPs, the electrical current along the graphene sheet is constant, that is, $|J(x)| = |\sigma(x)| \cdot |E_x(x)|$ = constant, leading to $|E_x(x)| \propto 1/|\sigma(x)|$. As for the other EM components of the

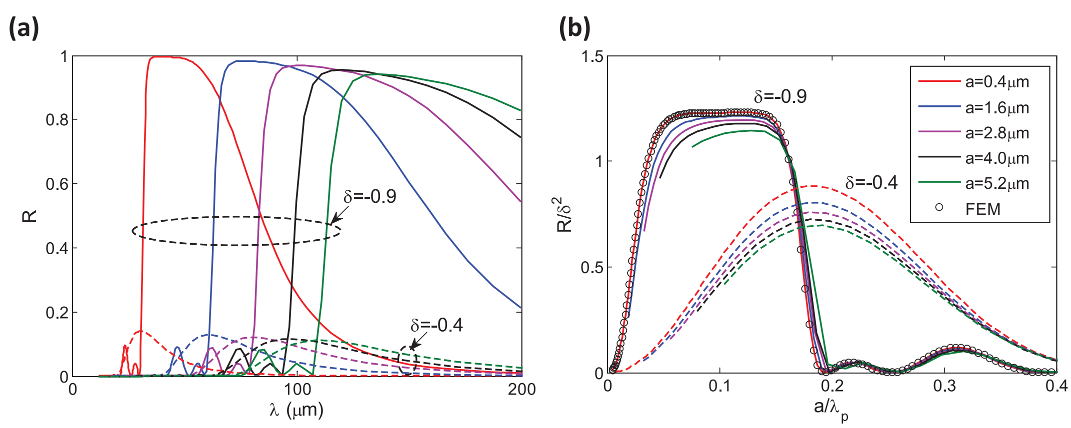

Figure 5. (a) Reflectance spectra for a GSP impinging a Gaussian conductivity defect, for different widths and for both δ **= −0.9 and** δ **= −0.4 . (b)** R/δ^2 **in function of** a/λ_p **for the same parameters considered in (a), showing the approximate scaling of the reflectance spectra. The open circles render calculations performed within the FEM (in order to validate those performed with the RPWE method), for** a **= 400 nm and** δ **= −0.9.**

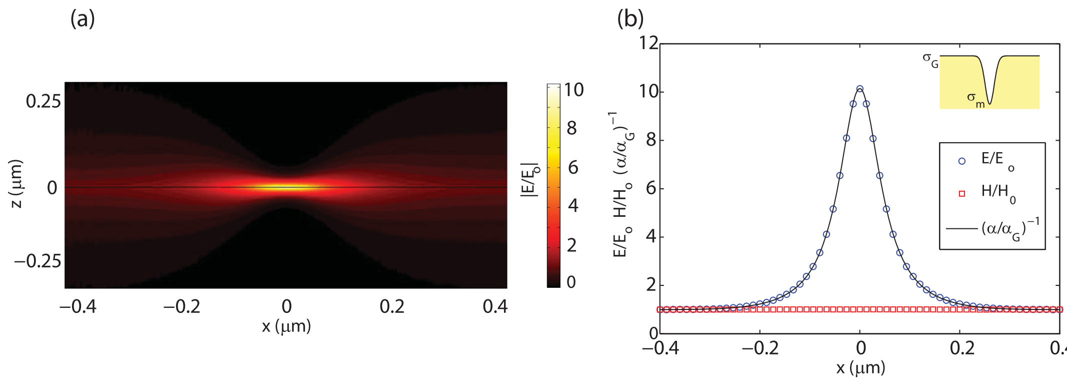

Figure 6. (a) Snapshot of the electric field norm along the GSP interacting with a Gaussian conductivity defect characterized by $\delta = -0.9$, defect width $a = 200$ nm and $\lambda = 10\,\mu$m. (b) Crosscut at $z = 0$ of the previous snapshot. Open squares represent the normalized magnetic field norm H/H_0 (open squares), which is approximately unity along the GSP propagation, and open blue circles render the normalized electric field norm E/E_0, showing the exact scaling with the inverse of normalized dimensionless conductivity $(\alpha/\alpha_G)^{-1}$ (continuous black line).

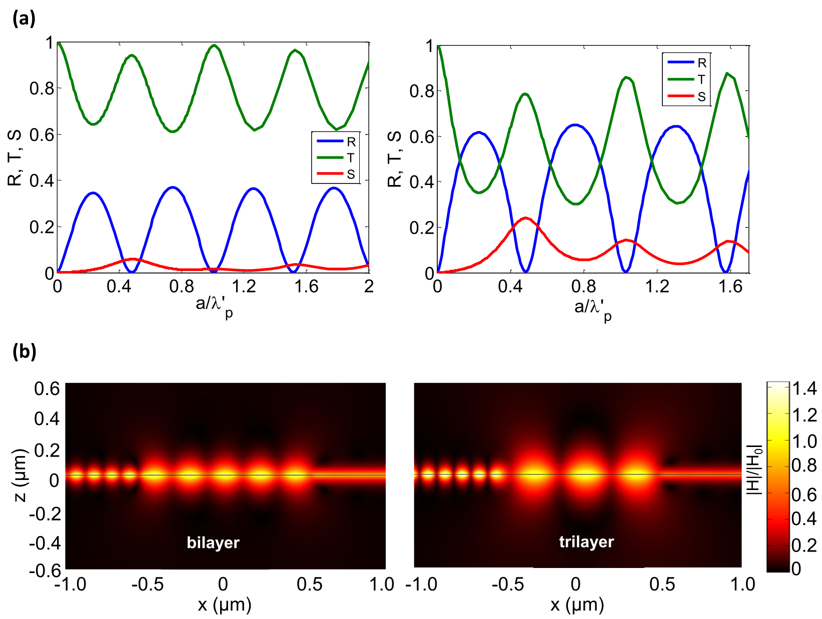

Figure 7. (a) Reflectance R, transmittance T, and fraction of energy radiated out-of-plane S for a GSP (free space wavelength $\lambda = 10\,\mu$m) impinging onto a strip of either bilayer (left) or trilayer (right) graphene. The scattering coefficients are presented as a function of strip size a (in units of the GSP wavelength in the island λ'_p, which for the considered case is 0.43 μm for the bilayer and 0.64 μm for the trilayer). (b) Snapshots of the magnetic field norm for a GSP propagating in a graphene monolayer and impinging onto either a bilayer (left) or a trilayer (right) strip of width $a = 1\,\mu$m.

GSP field, we know that they satisfy $|E_x| \simeq |E_z| \simeq |q_p H|$. So, taking into account that locally $q_p(x) \simeq i/\alpha(x)$, we arrive at $|H(x)| \simeq |\alpha(x) E_x(x)| \propto$ constant. The spatial dependence of the GSP field is rendered in Figure 6b, together with the conductivity profile, fully confirming the predicted scaling behavior.

Abrupt Defects. One paradigmatic case of defect with abrupt change in conductivity is an island of multilayer graphene, placed on a graphene monolayer. As for the small number of layers, the thickness of the multilayer is much smaller than the GSP extension along the normal to the sheet; this thickness can be neglected, and the multilayer region can be approximated by a conductivity defect. Here we analyze the scattering by both bi- and trilayer strips and approximate their conductivities as twice ($\delta = 1$) or three times ($\delta = 2$) the conductivity of a monolayer, respectively. The FOBA calculation for these rectangular-type defects gives $R^{\rm FOBA} = \sin^2(k_p a)\delta^2$, predicting that the reflectance spectra oscillates periodically when expressed as a function of a/λ_p. Within the FOBA, reflectance minima occur at $a = n\lambda_p/2, n = 1,2,...$ (which can be interpreted as the constructive interference in the backward direction between GSP partially reflected at the edges of the defect). The FOBA is not a good approximation for these defects where δ is not small, as it fails to take into account the modification in the GSP field inside the island due to the change in conductivity. However, we have found that the full calculations follow quite approximately the periodic behavior predicted by the FOBA, but as a function of a/λ'_p, where λ'_p is the

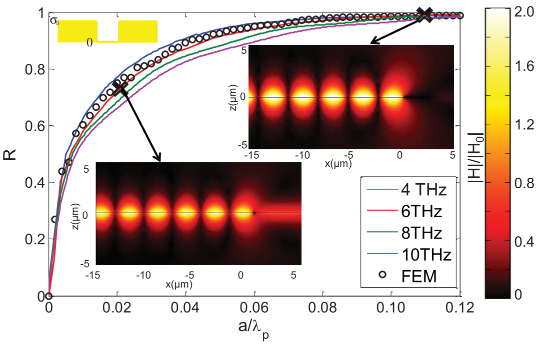

Figure 8. Reflectance *R* for a GSP impinging onto a crack, as a function of crack width *a*, for different frequencies. FEM calculation for 6 THz is shown to demonstrate the validity of the RPWE method. Inset: snapshots of the magnetic field norm, normalized to that of the incident magnetic field at the graphene sheet, for the cases $a/\lambda_p = 0.02$ and $a/\lambda_p = 0.11$.

wavelength of the plasmon corresponding to the conductivity inside the defect (see Figure 7a). Notice also that, for these abrupt defects, the scattering out-of-plane also presents an oscillatory behavior. Its amplitude, although smaller than the one for the reflectance, is not negligible and is peaked (as also does the transmittance) at the spectral positions where the reflectance is minimum.

As illustrated in Figure 7b, the strong reflection of GSP at the island boundaries results is the formation of standing waves in the island, with a number of nodes determined by both the island size and the GSP wavelength there. Notice that, as the conductivity inside the multilayer island is larger than in the monolayer, the GSP is less strongly bound to the graphene sheet. Also, Figure 7b clearly shows that the out-of-plane radiation is generated at the island boundaries. As a caveat, notice that Figure 7 considers a range of strip widths for which absorption of GSP may not be negligible. Nevertheless, full calculations assuming realistic values for the scattering time show that the lossless calculations provide the main features in the size dependence, being accurate for small a/λ_p' and semiquantitative for the largest strip widths considered (see Supporting Information).

Finally, as another paradigmatic case of abrupt defect, we study the scattering of a GSP by a crack in the graphene layer. The exact spatial dependence of the conductivity near the graphene edge is a question still under debate. However, the microscopic details of the graphene edge (whether has a zigzag or armchair configuration) play a role only for structures with sizes smaller than 10−20 nm.[45,46] Here we will simply assume that the conductivity vanishes within the gap region, in order to provide an estimation of the distances that GSP can tunnel through (calculations performed with an arbitrarily enhanced absorption in the 20 nm strips closer to the gap show that the reflectance spectra remains virtually unaltered; see Supporting Information). Figure 8 renders the dependence of the computed reflectance with gap width for several frequencies. The results are presented as function of a/λ_p, showing that the reflectance approximately follows a scaling behavior. Still, the reflectivity is high already for small values of a/λ_p, demonstrating the extreme sensitivity of GSPs to the presence of cracks in the graphene sheet. The insets to Figure 8 show snapshots of the magnetic field, illustrating (i) the standing wave arising from the reflection of the GSP at the crack, (ii) the smallness of the radiation out of the graphene sheet (in all calculations, the fraction of GSP energy radiated out-of-plane is $S \approx 10^{-3}$), and (iii) that, remarkably, a GSP is already substantially reflected for gaps as small as $0.01\lambda_p$ and fully reflected for $a > 0.1\lambda_p$.

CONCLUSION

We have analyzed the scattering properties of GSP by defects in the local conductivity of the graphene sheet. In the case of smooth spatial variations of the defect conductivity (which occur, for instance, when the defect is created by modification of the carrier concentration *via* a top gate), we have found that, for a given relative change in the conductivity at the defect center, the reflectance follows approximately a universal scaling in terms of a/λ_p. In all cases, the reflectance reaches its spectral maximum value when $a \approx 0.2\lambda_p$. When a/λ_p is larger than that given from the previous condition, the GSP propagation can be considered as adiabatic, and thus the GSP is mainly transmitted. When, additionally, the conductivity at the center of the defect is small, this leads to a strong electric field enhancement at the defect center. We have also found that, for these smooth defects, the scattering out-of-plane is always much smaller than the reflectance.

A different behavior is found for the scattering of GSP by multilayer islands, placed in a monolayer background. In this case, the scattering out-of-plane is not negligible, although on average it is smaller than the reflectance. In fact, the reflectance spectra oscillate periodically as a function of quotient between the island width and the plasmon wavelength *inside the defect*, with both transmittance and scattering out-of-plane presenting maxima at the reflectance minima.

Finally, we have found that conductivity gaps in the graphene sheet prevent very efficiently the GSP propagation, with the GSP being fully reflected for gap widths larger than $\sim 0.1\lambda_p$.

METHODS

Equation 2 has been solved discretizing q and replacing the infinite region of integration by increasingly larger finite limits, until convergency is achieved. A nonuniform discretization scheme in q-space is considered, in order to take into account the strong variations of the Green's function $G(q)$.[39,40]

Conflict of Interest: The authors declare no competing financial interest.

Acknowledgment. This work has been partially funded by the Spanish Ministry of Science and Innovation under Contracts MAT2011-28581-C02 and CSD2007-046-NanoLight.es.

Supporting Information Available: Additional figures and experimental details. This material is available free of charge *via* the Internet at http://pubs.acs.org.

Note Added after ASAP Publication. Due to a production error this paper was published on May 22, 2013 with incomplete images for Figures 3 and 4. The revised version was reposted on June 4, 2013.

REFERENCES AND NOTES

1. Bonaccorso, F.; Sun, Z.; Hasan, T.; Ferrari, A. C. Graphene Photonics and Optoelectronics. *Nat. Photonics* **2010**, *4*, 611–622.
2. Bao, Q.; Loh, K. P. Graphene Photonics, Plasmonics, and Broadband Optoelectronic Devices. *ACS Nano* **2012**, *6*, 3677–3694.
3. Grigorenko, A. N.; Polini, M.; Novoselov, K. S. Graphene Plasmonics. *Nat. Photonics* **2012**, *6*, 749–758.
4. Shung, K. W. K. Dielectric Function and Plasmon Structure of Stage-1 Intercalated Graphite. *Phys. Rev. B* **1986**, *34*, 979–993.
5. Hanson, G. Dyadic Green's Functions and Guided Surface Waves for a Surface Conductivity Model of Graphene. *J. Appl. Phys.* **2008**, *103*, 064302.
6. Jablan, M.; Buljan, H.; Soljačič, M. Plasmonics in Graphene at Infrared Frequencies. *Phys. Rev. B* **2009**, *80*, 245435.
7. Vakil, A.; Engheta, N. Transformation Optics Using Graphene. *Science* **2011**, *332*, 1291–1294.
8. Ju, L.; Geng, B.; Horng, J.; Girit, C.; Martin, M.; Hao, Z.; Bechtel, H.; Liang, X.; Zettl, A.; Shen, Y.; *et al.* Graphene Plasmonics for Tunable Terahertz Metamaterials. *Nat. Nanotechnol.* **2011**, *6*, 630–634.
9. 1Fei, Z.; Rodin, A. S.; Andreev, G. O.; Bao, W.; McLeod, A. S.; Wagner, M.; Zhang, L. M.; Zhao, Z.; Thiemens, M.; Dominguez, G.; *et al.* Gate-Tuning of Graphene Plasmons Revealed by Infrared Nano-Imaging. *Nature* **2012**, *487*, 82–85.
10. Chen, J.; Badioli, M.; Alonso-González, P.; Thongrattanasiri, S.; Huth, F.; Osmond, J.; Spasenovic, M.; Centeno, A.; Pesquera, A.; Godignon, P.; *et al.* Optical Nano-Imaging of Gate-Tunable Graphene Plasmons. *Nature* **2012**, *487*, 77–81.
11. Nikitin, A. Y.; Guinea, F.; Garcia-Vidal, F. J.; Martin-Moreno, L. Fields Radiated by a Nanoemitter in a Graphene Sheet. *Phys. Rev. B* **2011**, *84*, 195446.
12. Koppens, F. H. L.; Chang, D. E.; Garcia de Abajo, F. J. Graphene Plasmonics: A Platform for Strong Light–Matter Interactions. *Nano Lett.* **2011**, *11*, 3370–3377.
13. Velizhanin, K. A.; Efimov, A. Probing Plasmons in Graphene by Resonance Energy Transfer. *Phys. Rev. B* **2011**, *84*, 085401.
14. Gómez-Santos, G.; Stauber, T. Fluorescence Quenching in Graphene: A Fundamental Ruler and Evidence for Transverse Plasmons. *Phys. Rev. B* **2011**, *84*, 165438.
15. Hanson, G. W.; Yakovlev, A. B.; Mafi, A. Excitation of Discrete and Continuous Spectrum for a Surface Conductivity Model of Graphene. *Appl. Phys.* **2011**, *110*, 114305.
16. Thongrattanasiri, S.; Koppens, F. H. L.; Garcia de Abajo, F. J. Complete Optical Absorption in Periodically Patterned Graphene. *Phys. Rev. Lett.* **2012**, *108*, 047401.
17. Nikitin, A. Y.; Guinea, F.; Garcia-Vidal, F. J.; Martin-Moreno, L. Surface Plasmon Enhanced Absorption and Suppressed Transmission in Periodic Arrays of Graphene Ribbons. *Phys. Rev. B* **2012**, *85*, 081405.
18. Zhan, T. R.; Zhao, F. Y.; Hu, X. H.; Liu, X. H.; Zi, J. Band Structure of Plasmons and Optical Absorption Enhancement in Graphene on Subwavelength Dielectric Gratings at Infrared Frequencies. *Phys. Rev. B* **2012**, *86*, 165416.
19. Zhan, T. R.; Zhao, F. Y.; Hu, X. H.; Liu, X. H.; Zi, J. Enhanced Absorption of Graphene with One-Dimensional Photonic Crystal. *Appl. Phys. Lett.* **2012**, *101*, 052104.
20. Peres, N. M. R.; Ferreira, A.; Bludov, Y. V.; Vasilevskiy, M. I. Light Scattering by a Medium with a Spatially Modulated Optical Conductivity: The Case of Graphene. *J. Phys.: Condens. Matter* **2012**, *24*, 245303.
21. Manjavacas, A.; Nordlander, P.; Garcia de Abajo, F. J. Plasmon Blockade in Nanostructured Graphene. *ACS Nano* **2012**, *6*, 1724–1731.
22. Liu, P.; Cai, W.; Wang, L.; Zhang, X.; Xu, J. Tunable Terahertz Optical Antennas Based on Graphene Ring Structures. *Appl. Phys. Lett.* **2012**, *100*, 153111.
23. Tamagnone, M.; Gómez-Díaz, J. S.; Mosig, J. R.; Perruisseau-Carrier, J. Reconfigurable Terahertz Plasmonic Antenna Concept Using a Graphene Stack. *Appl. Phys. Lett.* **2012**, *101*, 214102.
24. Fang, Z.; Liu, Z.; Wang, Y.; Ajayan, P. M.; Nordlander, P.; Halas, N. J. Graphene-Antenna Sandwich Photodetector. *Nano Lett.* **2012**, *12*, 3808–3813.
25. Brey, L.; Fertig, H. A. Elementary Electronic Excitations in Graphene Nanoribbons. *Phys. Rev. B* **2007**, *75*, 125434.
26. Silvestrov, P. G.; Efetov, K. B. Charge Accumulation at the Boundaries of a Graphene Strip Induced by a Gate Voltage: Electrostatic Approach. *Phys. Rev. B* **2008**, *77*, 155436.
27. Popov, V. V.; Bagaeva, T. Y.; Otsuji, T.; Ryzhii, V. Oblique Terahertz Plasmons in Graphene Nanoribbon Arrays. *Phys. Rev. B* **2010**, *81*, 073404.
28. Nikitin, A. Y.; Guinea, F.; Garcia-Vidal, F. J.; Martin-Moreno, L. Edge and Waveguide Terahertz Surface Plasmon Modes in Graphene Microribbons. *Phys. Rev. B* **2011**, *84*, 161407.
29. Andersen, D. R.; Raza, H. Plasmon Dispersion in Semimetallic Armchair Graphene Nanoribbons. *Phys. Rev. B* **2012**, *85*, 075425.
30. Christensen, J.; Manjavacas, A.; Thongrattanasiri, S.; Koppens, F. H. L.; Garcia de Abajo, F. J. Graphene Plasmon Waveguiding and Hybridization in Individual and Paired Nanoribbons. *ACS Nano* **2012**, *6*, 431–440.
31. Wang, W.; Apell, P.; Kinaret, J. Edge Plasmons in Graphene Nanostructures. *Phys. Rev. B* **2011**, *84*, 085423.
32. Nagase, M.; Hibino, H.; Kageshima, H.; Yamaguchi, H. Local Conductance Measurements of Double-Layer Graphene on SiC Substrate. *Nanotechnology* **2009**, *20*, 445704.
33. Ahmad, M.; Han, S.; Tien, D.; Jung, J.; Seo, Y. Local Conductance Measurement of Graphene Layer Using Conductive Atomic Force Microscopy. *J. Appl. Phys.* **2011**, *110*, 054307.
34. Kim, K.; Artyukhov, V. I.; Regan, W.; Liu, Y.; Crommie, M. F.; Yakobson, B. I.; Zettl, A. Ripping Graphene: Preferred Directions. *Nano Lett.* **2012**, *12*, 293–297.
35. van der Zande, A. M.; Barton, R. A.; Alden, J. S.; Ruiz-Vargas, C. S.; Whitney, W. S.; Pham, P. H. Q.; Park, J.; Parpia, J. M.; Craighead, H. G.; McEuen, P. L. Large-Scale Arrays of Single-Layer Graphene Resonators. *Nano Lett.* **2010**, *10*, 4869–4873.
36. Lemme, M.; Koppens, F.; Falk, A.; Rudner, M.; Park, H.; Levitov, L.; Marcus, C. Gate-Activated Photoresponse in a Graphene p–n Junction. *Nano Lett.* **2011**, *11*, 4134–4137.
37. Gorbachev, R. V.; Mayorov, A. S.; Savchenko, A. K.; Horsell, D. W.; Guinea, F. Conductance of p-n-p Graphene Structures with "Air-Bridge" Top Gates. *Nano Lett.* **2008**, *8*, 1995–1999.
38. Liu, G.; Jairo Velasco, J.; Bao, W.; Lau, C. N. Fabrication of Graphene p-n-p Junctions with Contactless Top Gates. *Appl. Phys. Lett.* **2008**, *92*, 203103.
39. Sánchez-Gil, J. A.; Maradudin, A. A. Near-Field and Far-Field Scattering of Surface Plasmon Polaritons by One-Dimensional Surface Defects. *Phys. Rev. B* **1999**, *60*, 8359–8367.
40. Nikitin, A. Y.; López-Tejeira, F.; Martín-Moreno, L. Scattering of Surface Plasmon Polaritons by One-Dimensional Inhomogeneities. *Phys. Rev. B* **2007**, *75*, 035129.
41. Comsol Multiphysics, http://www.comsol.com/.
42. Wunsch, B.; Stauber, T.; Sols, F.; Guinea, F. Dynamical Polarization of Graphene at Finite Doping. *New J. Phys.* **2006**, *8*, 318.
43. Hwang, E. H.; Das Sarma, S. Dielectric Function, Screening, and Plasmons in Two-Dimensional Graphene. *Phys. Rev. B* **2007**, *75*, 205418.
44. Falkovsky, L. A. Optical Properties of Graphene and IV–VI Semiconductors. *Phys.-Usp.* **2008**, *51*, 887.
45. Owens, F. J. Electronic and Magnetic Properties of Armchair and Zigzag Graphene Nanoribbons. *J. Chem. Phys.* **2008**, *128*, 194701.
46. Thongrattanasiri, S.; Manjavacas, A.; Garcia de Abajo, F. J. Quantum Finite-Size Effects in Graphene Plasmons. *ACS Nano* **2012**, *6*, 1766–1775.